JOURNAL OF GEOPHYSICAL RESEARCH, VOL. 105, NO. A12, PAGES 27,739–27,754, DECEMBER 1, 2000

Modeling the inner magnetosphere: The asymmetric ring current and Region 2 Birkeland currents revisited

N. A. Tsyganenko [1]

Laboratory for Extraterrestrial Physics, NASA Goddard Space Flight Center, Greenbelt, Maryland

Abstract. A quantitative model is developed of the inner magnetospheric magnetic field, combining the effects of the azimuthally asymmetric ring current with those of field-aligned currents, due to azimuthal variation of the plasma pressure. The axisymmetric part of the model ring current was derived from average observed radial profiles of the particle pressure and anisotropy and was analytically represented by a vector potential, fitted by least squares to one derived by the Biot-Savart integral. The contribution of the asymmetric part, including the field of Birkeland currents, closed via the ionosphere, was represented as a divergenceless combination of expansions for the components of the **B** vector, and was also fitted by least squares to the corresponding Biot-Savart field. The total field-aligned current, associated with the noon-midnight pressure asymmetry of the outer ring current, was found to be significantly smaller than the total Region 2 current, observed at low altitudes. It is therefore concluded that most of that current is generated in the near-Earth plasma sheet. The goal of this work is a realistic and computationally efficient description of the asymmetric ring current, to be included in an advanced model of the external geomagnetic field.

1. Introduction

The inner magnetosphere can be viewed as a focal region of the near-Earth space, where the storm time radiation belts of charged particles are formed, energized, and eventually dissipated in the upper atmosphere. The ongoing rapid expansion of human activities into near-Earth space creates a need for more accurate dynamical models of the inner magnetosphere, already emphasized in many studies [e.g., *Nakabe et al.*, 1997].

The principal external contribution to the inner geomagnetic field comes from the ring current and from a system of field-aligned currents, which closes the asymmetrical part of the ring current via the ionosphere. Since the discovery of the radiation belts in the late 1950s, the composition, energy spectra, and spatial distribution of the ring current particles were widely studied, using abundant experimental data and increasingly sophisticated models (see reviews by *Williams* [1983] and a more recent one by *Daglis et al.* [1999]). However, very few of those studies took the additional step of calculating the electric currents and estimating the associated magnetic field disturbance. In fact, no major progress was seen in that direction after the first decade of active studies, pioneered by *Akasofu and Chapman* [1961] and followed by other modeling efforts [e.g., *Hoffman and Bracken*, 1965, 1967; *Sozou and Windle*, 1969; *Lackner*, 1970; *Sckopke*, 1972]. *Lui et al.* [1987] and *Lui and Hamilton* [1992] (hereinafter referred to as LH92) obtained the equatorial volume density of the ring current, based on data of AMPTE/CCE spacecraft; however, no attempt was made to derive the associated magnetic field.

In terms of the modeling, the problem requires more than just the numerical evaluation of the magnetic field by the Biot-Savart integral. Most experimental and theoretical studies require compact and flexible analytical models, valid within a wide range of altitudes from the ionosphere to the distant magnetosphere. Somewhat surprisingly, during almost four decades of the magnetospheric studies, just a few models of that kind were proposed, virtually all of them limited to the case of an axially symmetric ring current. *Kendall et al.* [1966] suggested using a flux function Ψ, related to the azimuthal component of the vector potential A_ϕ, and they provided tables of the first three coefficients in the expansions of Ψ in associate Legendre polynomials. *Schield* [1969] published another tabular representation for the components of the field of an axially symmetric ring current, covering the interior of a sphere $R = 13\,R_E$. That approach was further developed by *Sckopke* [1972], and *Voigt* [1981] introduced the Sckopke's ring current into his model of the magnetosphere (neither ring current model was ever published).

A different, purely empirical method of modeling the ring current was developed by *Tsyganenko and Usmanov* [1982]. In that approach, no assumptions were made about the spatial and pitch angle distribution of the ring current particles. Instead, a simple mathematical representation for the vector potential was proposed from the outset, and an attempt was made to deduce the field and the current from the magnetometer data, rather than to calculate them from particle measurements or models. That kind of model was also used by *Hilmer and Voigt* [1995], who added a second inner cur-

[1] Also at Raytheon Information, Technology, and Scientific Services Corporation, Lanham, Maryland.

Paper number 2000JA000138.
0148-0227/00/2000JA000138$09.00

rent, to replicate the effect of the eastward diamagnetic currents due to the earthward decrease of the particle pressure at close distances. *Kosik* [1989, 1998] suggested a simple empirical approximation for the ring current, using poloidal vector fields. In the most recent global magnetosphere model [*Tsyganenko,* 1996] the axisymmetric part of the ring current was represented by a spread-out current disk with a variable thickness, based on simple analytical expansions for the vector potential by *Tsyganenko and Peredo* [1994].

Axially symmetric models, however, provide only a crude approximation of the actual ring current. Both observations and numerical simulations reveal a significant asymmetry. *Iijima et al.* [1990] found the nightside azimuthal currents to exceed the dayside ones by a factor between 2 and 3, on the basis of a statistical study of AMPTE/CCE data for prolonged disturbed periods. Using more than 3000 days of the DE 1 magnetometer data, *Nakabe et al.* [1997] also found pronounced noon-midnight and dawn-dusk asymmetries in the inner magnetosphere, which remained appreciable even under quiet geomagnetic conditions. A similar result was obtained in LH92 and in our recent study [*Tsyganenko et al.,* 1999], based on Polar magnetometer measurements at low latitudes.

The azimuthal asymmetry of the ring current necessarily implies the existence of Birkeland currents, closing the diverging part of the azimuthal drift current via the ionosphere. The excess of westward current on the nightside suggests a field-aligned current having the sense of Region 2, that is, downward (upward) on the evening side (morning side). This scenario was conjectured by *Iijima et al.* [1990] from their study of the equatorial field, and it was corroborated by *Nakabe et al.* [1997].

Global modeling of the magnetic field of the asymmetric ring current still remains an almost untouched area. To our knowledge, the first consistent efforts to bridge the gap were described by *Tsyganenko* [1993] (hereinafter referred to as T93) and by *Stern* [1993]. In their works, the model ring and field-aligned currents were not spread out in space but flowed on an infinitely thin dipolar L shell. Although both models yielded reasonable fields away from that partial ring current shell, they left much room for improvement, because of the unphysically narrow radial extent of the region, occupied by the current.

In a later work by the same authors [*Tsyganenko and Stern,* 1996] the model partial ring current was spread out over a finite interval of radial distance; however, its spatial configuration was not derived from any trapped plasma distribution but was postulated empirically. In addition, the model field was specified separately in three domains. In the low- and high-latitude regions (outside of the spread-out current) it was represented by sophisticated combinations of harmonic functions, while inside the current layer each component of the magnetic field was approximated by lengthy (80-term) expansions. The partial ring current field of *Tsyganenko and Stern* [1996] was used in a global data-based magnetosphere model [*Tsyganenko,* 1996].

Another attempt to model the partial ring current was made by *Peroomian et al.* [1998], who used a "wire" approximation. In that work the partial ring current was regarded as a way to close the observed Region 2 Birkeland system at the equator. Here, in contrast, we treat the field-aligned currents in an opposite perspective, i.e., as the closure currents for the partial ring current, obtained from the observed asymmetry of the equatorial pressure.

In the present work we revisit the approach developed in T93, aiming at a more realistic and mathematically simpler model of the asymmetric ring current. We start by defining a model of the ring current particle distribution in a dipolar magnetic field, from which the associated electric currents are then derived. Unlike in T93, the ring current in the present model covers a wide interval of the L parameter and has a realistic radial profile of trapped particle pressure and pitch angle anisotropy, based on the results of LH92 obtained from the data of AMPTE/CCE.

We also assumed the simplest form of the local time variation of the particle pressure, consisting of a constant term and one proportional to the cosine of the solar magnetic longitude. As in T93, this allowed us to separate the total electric current and magnetic field into two parts, corresponding to an axisymmetric ring current and a "quadrupole" part, in which the local time variation of all related quantities also obeys the simplest sine (or cosine) dependence. This reduces the dimensionality of the problem from 3 to 2, so that it suffices to calculate and analytically approximate the fields in only one meridional plane.

Following the above outline, the paper is organized as follows. Section 2 formulates the problem and describes the numerical procedure of the magnetic field calculation. Section 2.1 treats the symmetrical part of the ring current, based on particle characteristics obtained in LH92 and describes an analytical approximation for the corresponding magnetic field. Section 2.2 addresses the field of the partial ring current, responsible for the azimuthal asymmetry, and presents analytical approximations for its symmetric and quadrupole parts. Section 3 discusses the results and their possible extensions in the future models.

2. Asymmetric Ring Current: Spatial Configuration and Calculation of the Global Magnetic Field

To obtain the spatial distribution of the electric current, we need first to define the transverse and field-aligned pressures $p_\perp$ and $p_\parallel$ as functions of the position $\mathbf{r}$. The volume current density is then derived from $p_\perp(\mathbf{r})$ and $p_\parallel(\mathbf{r})$, assuming a purely dipolar magnetic field. In other words, we neglect the distortion produced by external field sources, including the ring current itself. This assumption will be further discussed in section 3.

The adopted spatial distribution of $p_\perp$ and $p_\parallel$ is based on the following observational facts, established in LH92: (1) In the inner magnetosphere, roughly between ~ 2 and $\sim 5\,R_E$, the quiet time ring current is virtually axisymmetric, while beyond that region a significant noon-midnight asymmetry exists, rapidly increasing with growing distance. (2) The transverse pressure $p_\perp$ is significantly larger than the parallel one $p_\parallel$ in the innermost ring current; however, the anisotropy rapidly decreases with the distance, so that for $r \geq 6$ one may assume $p_\perp \approx p_\parallel$.

In view of these observations we construct a model which superposes a fully symmetrical ring current (SRC), with the radial profiles of $p_\perp$ and $p_\parallel$ based on those from LH92, and a partial ring current (PRC), whose current density peaks at a larger distance on the nightside. Section 2.1 concentrates on the SRC, while the PRC model will be treated in section 2.2.

2.1. Modeling the Symmetrical Ring Current

Figure 1 shows the radial variation of the transverse pressure $p_{\perp e}$ in the equatorial plane, where the observed values correspond to the quiet time profile of LH92 (their Figure 7; note also that we use a linear scale for the pressure, in contrast to the logarithmic one in LH92). A model approximation was obtained as a least squares fit to the observed values, using the following function of the equatorial radial distance r_e:

$$p_{\perp e} = \begin{cases} p_m \cos^2\left(\frac{\pi}{2}\frac{r_m - r_e}{r_m - r_1}\right) \exp\left[-\left(\frac{r_m - r_e}{\Delta r_1}\right)^2\right] \\ \qquad r_1 \le r_e \le r_m\,, \\ p_m \cos^2\left(\frac{\pi}{2}\frac{r_m - r_e}{r_m - r_2}\right) \sqrt{1 + \left(\frac{r_m - r_e}{\Delta r_1}\right)^2} \\ \qquad r_m \le r_e \le r_2\,, \\ 0 \qquad r_e < r_1 \text{ or } r_e > r_2\,, \end{cases} \tag{1}$$

where p_m is the peak pressure and r_m is the distance at which it occurs. The model profile (equation (1)) describes a steep earthward falloff of $p_{\perp e}$ on the inner side of the SRC and a more gradual decrease on the outer side. The cosine factors in (1) ensure a smooth transition to zero pressure at the inner and outer boundaries of the SRC, assumed to be at equatorial distances $r_1 = 1.6\,R_E$ and $r_2 = 8.0\,R_E$, respectively. The best fit values for the variable parameters in (1) are $p_m = 20.494$ nPa, $r_m = 2.8391$, $\Delta r_1 = 0.7081$, and $\Delta r_2 = 0.6937$.

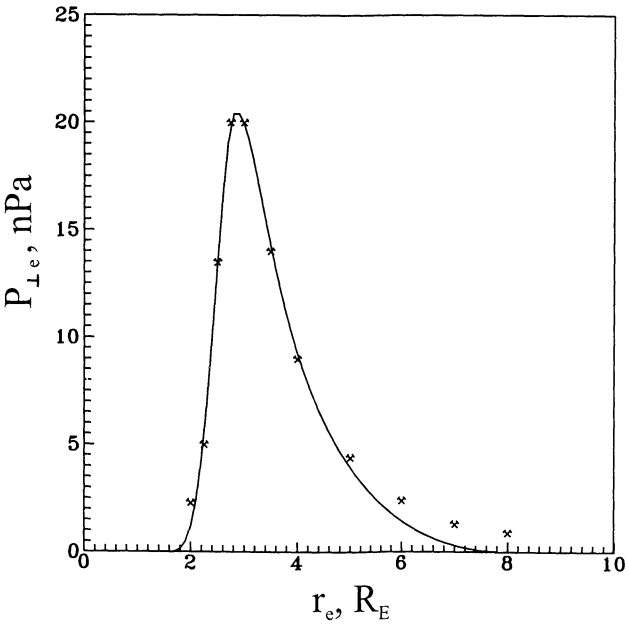

Figure 1. Radial profile of the transverse pressure $p_{\perp e}$ in the equatorial plane. The observed values (crosses) were taken from LH92, while the best fit model approximation (solid line) is given by equation (1), representing only the axisymmetric part of the ring current (this is why the outermost part of the model profile deviates from the experimental points).

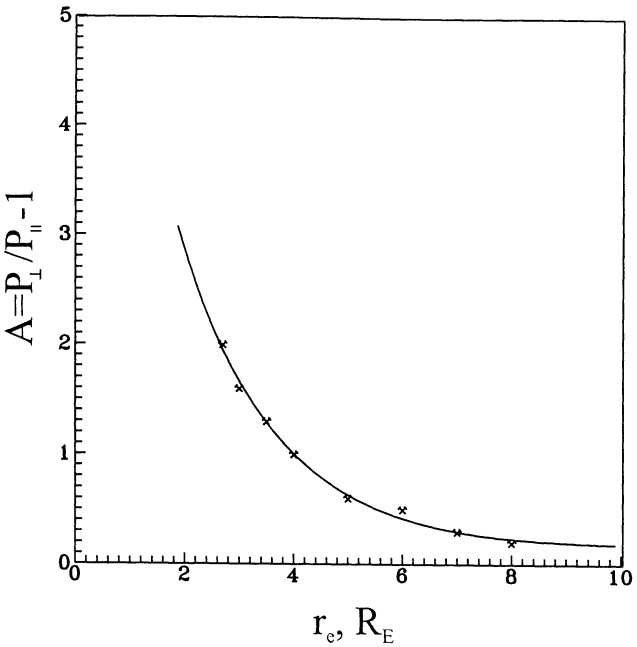

Figure 2. Radial profile of the equatorial pressure anisotropy parameter A, defined by equation (2). The observed values (crosses) were taken from LH92, and the best fit approximation (equation (3)) is shown by a solid line.

Note that the model profile of $p_{\perp e}$ gradually deviates from the measured values for $r_e > 5\,R_E$, and unlike the observed pressure, it falls off to zero at the outer boundary. This is because the model profile (equation (1)) only represents the axisymmetric part of the ring current, while the measured values give the total pressure. The remaining difference between them is contributed by the PRC and by the inner part of the tail plasma sheet; that component will be addressed separately in section 2.2.

The parallel pressure $p_{\parallel e}$ in the equatorial plane can be obtained from the transverse one given by (1), provided the anisotropy parameter

$$A(r_e) = \frac{p_{\perp e}}{p_{\parallel e}} - 1 \tag{2}$$

is known. This parameter was derived from the AMPTE/CCE data in LH92, and *Lui et al.* [1994] also gave an analytical approximation for $A(r_e)$ by a fifth-order polynomial of r_e. In this work we used the observed values of $A(r_e)$ from LH92; however, instead of fitting them to a polynomial, we assumed a simpler exponential approximation,

$$A(r_e) = a + b\exp(-r_e/c)\,, \tag{3}$$

with the following best fit values of the parameters: $a = 0.1561$, $b = 8.632$, and $c = 1.7212$. The observed values and the model profile of $A(r_e)$ are shown in Figure 2.

Having thus defined the equatorial pressures $p_{\perp e}$ and $p_{\parallel e}$, one can derive the pressure distribution everywhere in space, once a background magnetic field model is specified and certain assumptions are made with regard to the pitch angle distribution function. As already mentioned, in this work we assume a purely dipolar background field, and we calculate the currents in the "low-beta" approximation; that is, we neglect the field of the ring current itself.

With regard to the particle pitch angle distribution, two kinds of the distribution function allow a simple and straightforward calculation of the pressure variation along field lines. The first one, suggested by *Parker* [1957] and used in a ring current model by *Akasofu and Chapman* [1961], represents the dependence on the pitch angle Θ via a factor $\sin^{\beta+1}\Theta$. In this case both $p_\perp$ and $p_\parallel$ vary with the magnetic field strength B along the field lines as $B^{-\beta/2}$, and hence the anisotropy factor A is constant along the magnetic field, remaining equal to $\beta/2$. In the case of a purely dipolar field the ratio

$$\frac{B_e}{B} \equiv S = \frac{\sin^6\theta}{\sqrt{1+3\cos^2\theta}} \tag{4}$$

(where θ is the dipole colatitude) determines the pressure variation along a field line as

$$p_\perp = p_{\perp e}(r_e)\, S^{A(r_e)}, \qquad p_\parallel = \frac{p_\perp(r_e)}{A(r_e)+1}, \tag{5}$$

where $r_e = r/\sin^2\theta$ is the equatorial radius of the field line.

A second type of distribution allowing a simple derivation of the pressures is the bi-Maxwellian function, discussed in detail by *Cowley* [1978] and used by *Spence et al.* [1987]. In that case,

$$p_\perp = p_{\perp e}(r_e)G, \qquad p_\parallel = p_{\parallel e}(r_e)\sqrt{G}, \tag{6}$$

where, using (4),

$$G = \frac{1}{[1+A(r_e)(1-S)]^2}. \tag{7}$$

Relations (1)–(7), combined with the well-known formula

$$\mathbf{j} = \frac{c}{B^2}\mathbf{B}\times\left(\nabla p_\perp + \frac{p_\parallel - p_\perp}{\rho_c}\mathbf{e}_c\right), \tag{8}$$

where $\mathbf{e}_c/\rho_c$ is the field line curvature, complete the set of equations necessary for calculating the electric current at any location.

Figure 3 shows distributions of the volume current density in a meridional plane, calculated with Parker's and bi-Maxwellian distribution functions, based on the same equatorial profile of $p_{\perp e}$ and anisotropy function $A(r_e)$, adopted from LH92. For comparison, the right panel shows the result, obtained with the same radial pressure profile but assuming fully isotropic pitch angle distribution. The total westward current in the outer part of the ring current varied between 0.75 MA for the bi-Maxwellian case and 0.85 MA for the isotropic case, while the inner eastward current was found equal to 0.023 MA for the anisotropic cases and tripled up to 0.069 MA in the isotropic case. Note that these results correspond to a quiet time ring current, based on the data of LH92.

As it should be, in the isotropic case the particle pressure and hence the transverse electric current extend far along the field lines, while for the actually observed anisotropy they remain concentrated relatively close to the equator. As shown by *Sckopke* [1972], in the self-consistent model the field of the ring current itself would weaken the total equatorial field and hence confine the near-equatorial current to an even narrower layer. So, using a realistic radial profile of the particle pressure, peaked relatively close to Earth and gradually decreasing outward, and taking into account the observed anisotropy, results in a remarkably near-equatorial disk-like ring current, extending deep into the inner magnetosphere. This is exactly what *Sugiura* [1972] obtained from the data on the distribution of the scalar difference $\Delta B = B - B_{\mathrm{IGRF}}$, and he pointed out that his observation contradicted models of the ring current used at that time. This also supports our choice of the disk-like model ring current by *Tsyganenko and Peredo* [1994] used in the T96 model.

Once the current density is assumed, we can proceed to the calculation of the vector potential, given by the Biot-Savart integral,

$$\mathbf{A} = \frac{1}{c}\int \frac{\mathbf{j}(\mathbf{r}')dv}{|\mathbf{r}-\mathbf{r}'|}. \tag{9}$$

In a cylindrical coordinate system $\{\rho, \phi, z\}$, the potential (equation(9)) of the axially symmetric ring current has only one nonzero component, A_ϕ. In principle, owing to the ax-

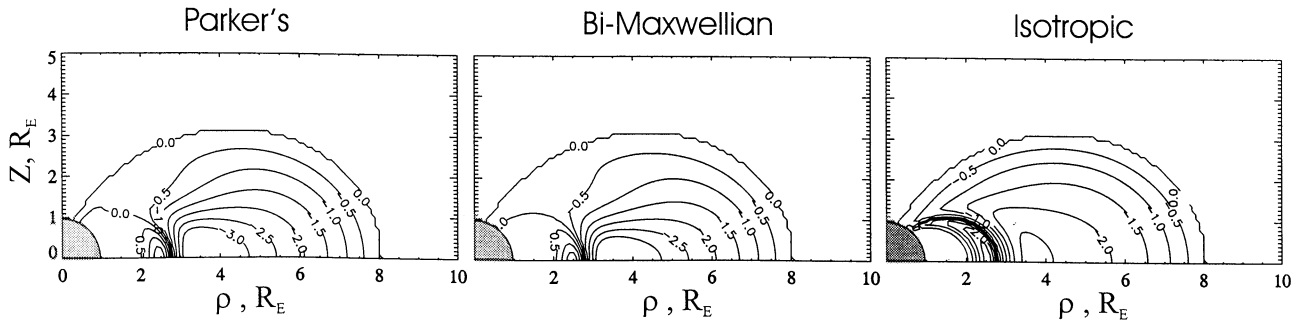

Figure 3. Distribution of the volume current density j in model ring currents for three choices of the pitch angle distribution function: (left) Parker's function $\sim \sin^{\beta+1}\Theta$, (middle) bi-Maxwellian one, and (right) isotropic distribution. The lines of equal intensity of j are labeled in nanoamperes per square meter.

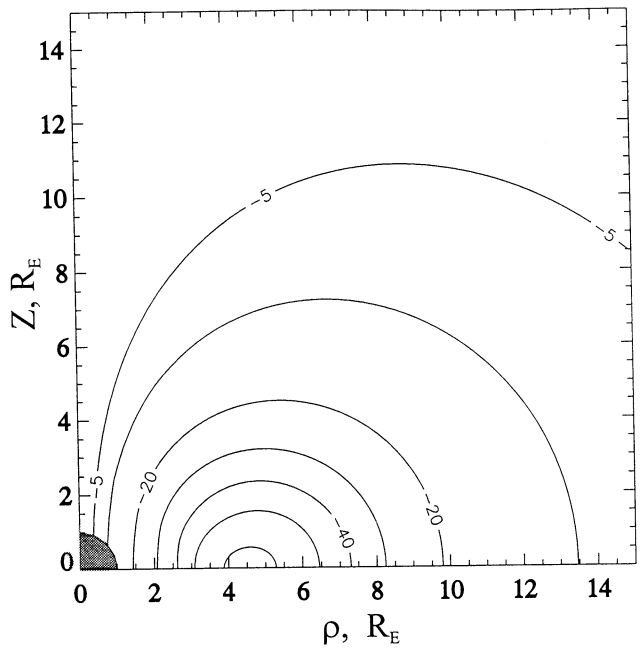

Figure 4. Distribution of the azimuthal component A_ϕ of the vector potential, corresponding to the profiles of the quiet time particle pressure and the pressure anisotropy in the axially symmetrical part of the model ring current, given in Figures 1 and 2, and to the bi-Maxwellian particle distribution function (equations (6) and (7)). This vector potential was obtained as the Biot-Savart integral (equation (9)) with the electric current given by equation (8) (Figure 3, middle). The lines of equal A_ϕ are labeled in units of nT·R_E.

ial symmetry, one can perform the integration in only two dimensions, representing the entire ring current by a set of circular loops, as was done, for example, by *Akasofu and Chapman* [1961]. However, in preparation for the computation of the partial ring current model, where (unlike here) the Biot-Savart integral cannot be reduced to two dimensions, we preferred to carry out the integration in three dimensions, so that the same algorithm could be used later for the partial ring current model (described in section 2.2).

The entire volume occupied by the ring current was divided into 50 layers bounded by 51 dipolar L shells and corresponding to 50 equal intervals of the footpoint colatitude. Each layer was divided by meridional cuts into a number of sectors, so that the cross sections of the resulting field line tubes were, on the average, as close as possible to squares. Finally, each field line tube was divided into volume elements, choosing their dimensions along **B**, so that their shapes were as close as possible to cubes. The total number of volume elements in the numerical integration was $N = 1,166,499$. Special care was taken of the singularities of the integrand by replacing $|\mathbf{r}-\mathbf{r}'| \to \sqrt{|\mathbf{r}-\mathbf{r}'|^2 + D^2}$, with $D = \Delta V^{1/3}$, i.e., not allowing it to become smaller than the linear size of the volume element.

Figure 4 shows the distribution in a meridian plane of the potential A_ϕ, derived from the LH92 quiet time particle pressure profile; Figure 5 presents the corresponding plots for the field components B_ρ and B_z, numerically computed from the potential in Figure 4. As already stressed in section 1, a major challenge was to find a convenient analytical approximation for that field; a simple solution was found and is given below.

The idea was to start from a crude and very simple model, representing the ring current by a pair of spread-out current loops [*Tsyganenko*, 1998a], and then to deform the coordinates, adjusting the deformation parameters and the amplitudes of the current loops to fit the actual distribution of the vector potential. The initial undeformed potential was defined as

$$A_\phi^{(0)} = \sum_{i=1}^{2} a_i \frac{(1-k_i^2/2)K(k_i) - E(k_i)}{k_i \rho^{1/2}}, \qquad (10)$$

where

$$k_i^2 = \frac{4\rho_i \rho}{(\rho_i+\rho)^2 + z^2 + D_i^2},$$

and where K and E are complete elliptical integrals of the second and first kind. This initial model has six variable parameters, including two amplitude coefficients a_1 and a_2, the loop radii ρ_1 and ρ_2, and their spatial spreads D_1 and D_2.

Since the geometry of the ring current is closely related to the configuration of the background magnetic field, it was not too surprising that a relatively simple deformation of the dipolar orthogonal coordinates,

$$\alpha = \frac{\sin^2\theta}{r}, \quad \gamma = \frac{\cos\theta}{r^2}, \qquad (11)$$

yielded an accurate approximation. Given a point $\{\rho, z\}$ in space, we derived $\{\alpha, \gamma\}$ and then deformed α to

$$\alpha' = \alpha\left\{1 + \sum_{i=1}^{3} p_i \exp\left[-\left(\frac{r-r_i}{\Delta r_i}\right)^2 - c_i\cos^2\theta\right]\right\}. \qquad (12)$$

After that, transforming $\{\alpha', \gamma\}$ back to deformed cylindrical coordinates $\{\rho', z'\}$ (the transformation itself is described in the next paragraph), and using the latter coordinates instead of $\{\rho, z\}$ in (10), yielded a very accurate approximation to the exact vector potential (equation (9)). A least squares fitting of the parameters, entering in (10) and (12), was performed by using a simplex minimization code over the region $\rho \le 15\,R_E$, $0 \le z \le 15\,R_E$, excluding the Earth's interior $(\rho^2 + z^2)^{1/2} \le 1\,R_E$. In total, the model (equations (10)–(12)) has 18 variable parameters, whose best fit values are given in Table 1. The quality of approximating the exact vector potential by (10)–(12) can be gauged by the ratio σ of the rms deviation δA_ϕ to the rms potential $\langle A_\phi^2\rangle^{1/2}$; its best-fit value was σ=0.5%.

The inverse transformation from the dipolar coordinates (equation (11)) to standard spherical or cylindrical ones is not quite obvious, but it is completely analytical. It was described in our earlier work (T93, Appendix A), and for the sake of completeness it is reproduced in brief below. For any α and γ, define

$$f = \frac{64}{27}\gamma^2 + \frac{\alpha^4}{4}, \quad Q = \left(\sqrt{f} + \frac{\alpha^2}{2}\right)^{1/3},$$
$$c = Q - \frac{4}{3}\frac{|\gamma|^{2/3}}{Q}, \quad g = \sqrt{c^2 + 4|\gamma|^{2/3}}; \qquad (13)$$

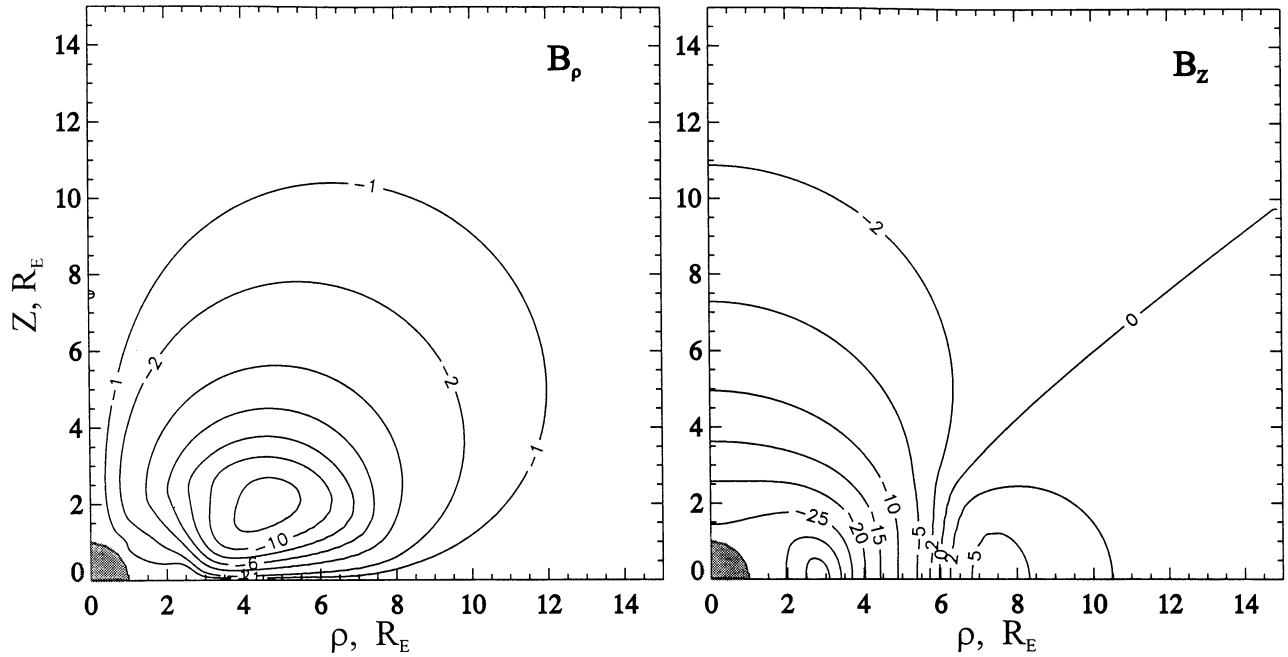

Figure 5. Distribution of the magnetic field components B_ρ and B_z produced by the axisymmetrical model ring current, corresponding to the numerically computed vector potential in Figure 4. The lines of equal B_ρ and B_z are labeled in nanotesla.

then the spherical coordinates are readily obtained from

$$r = \frac{4}{(\sqrt{2g - c} + \sqrt{c})(g + c)}, \qquad \cos\theta = \gamma r^2 . \qquad (14)$$

The components of the magnetic field in either the spherical or the cylindrical coordinate system can be easily derived from (10)–(13) by applying the curl operation, either analytically or numerically. Figure 6 displays the model field components B_ρ and B_z in cylindrical coordinates; comparing them visually with the similar plots for the exact solution in Figure 5 does not reveal any significant difference. The close agreement between the model and the original Biot-Savart field appears even more striking in Figure 7, where the initial electric current distribution (Figure 3, middle) is compared to the one derived as $c/4\pi \nabla \times \nabla \times \mathbf{A}$ from the model vector potential (equations (10)–(13)). In spite of applying

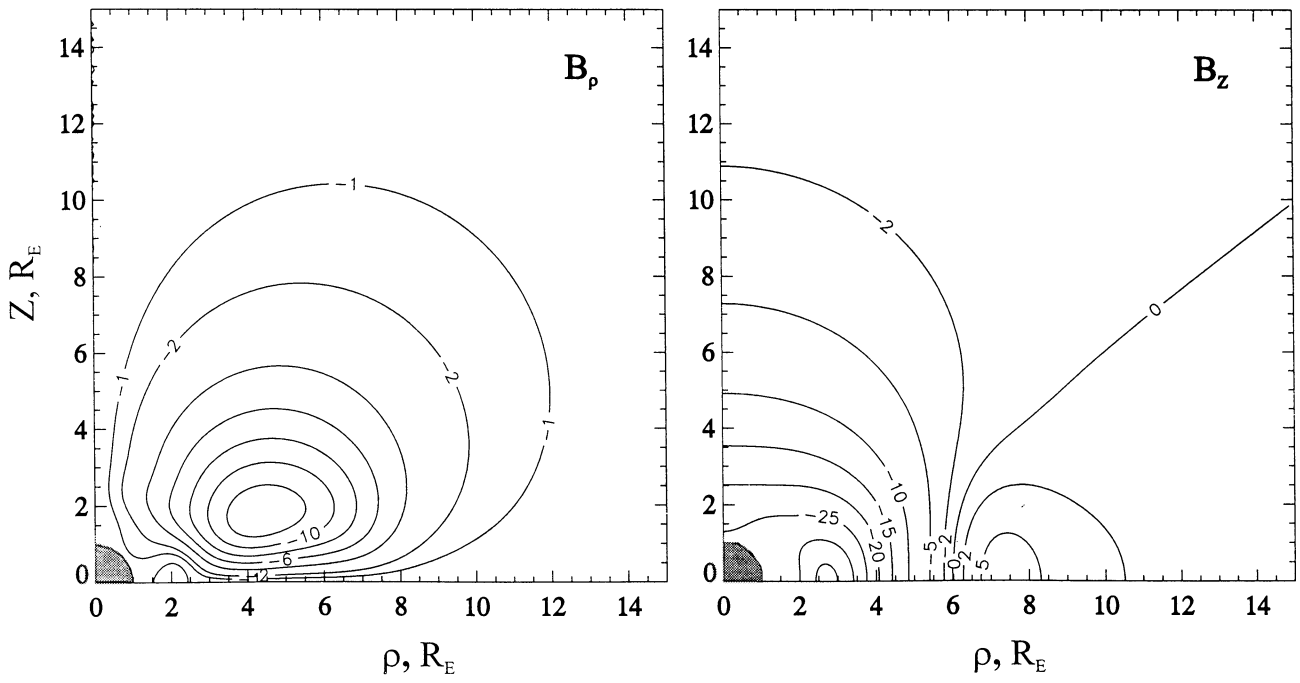

Figure 6. Equal intensity plots for B_ρ and B_z, obtained from the analytical approximation (equations (10)–(12)) for the model vector potential. Compare with Figure 5.

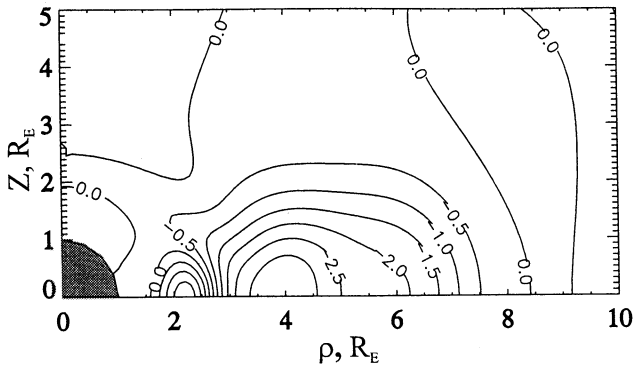

Figure 7. Distribution of the volume density of the electric current, computed from the analytical model (equations (10)–(12)) of the vector potential for the axisymmetrical part of the ring current. Compare to the original electric current distribution (Figure 3, middle), used in the Biot-Savart integral (equation (9)).

twice the curl operation (which often produces large discrepancies between the initially assumed and model currents), in this case the model current distribution closely resembles the one we have started with.

2.2. Modeling the Partial Ring Current and Associated Birkeland Currents

The PRC model is based on the following observations and assumptions. First, we again assume a purely dipolar background magnetic field.

Second, as mentioned in section 2.1, we adopt the finding of LH92, that the noon-midnight asymmetry of the ring current becomes significant beyond equatorial distances $\sim 5\ R_E$ and rapidly increases outward. A larger particle energy density on the nightside implies an azimuthal variation of the westward drift current and hence its redirection into the Region 2 Birkeland current.

Third, at sufficiently large tailward distances the particle population of the ring current gradually merges with that of the tail plasma sheet. Beyond a distance of $R = 7 - 8\ R_E$ on the nightside, the equatorial current flow lines no longer encircle Earth but reach the magnetopause and close there, which corresponds to the transition from the ring current to the cross-tail current system. This boundary can be taken as a rough estimate of the outward limit of the PRC (although the poleward part of the Region 2 currents is partially fed by the diverging cross-tail current as well).

Fourth, as shown in LH92, the pressure anisotropy becomes rather small beyond $\sim 5 - 6\ R_E$, making it reasonable to assume that the PRC plasma is isotropic. That assumption allows one to specify the pressure p as a function of only two variables, α and the solar magnetic longitude ϕ.

Fifth, we assume that the local time variation of pressure is rather smooth and can be approximated by a simple cosine modulation factor, as specified in section 2.2.2. This greatly simplifies the problem, since, as shown in T93 (Appendix B), any individual Fourier term with $\cos m\phi$ or $\sin m\phi$ in the expansion for the pressure $p(\alpha, \phi)$ gives rise to only one term of the same order in a similar expansion for the magnetic field components. For that reason, it suffices to model either spherical or cylindrical components of B in only one meridional plane, since their values at any other local time can be easily obtained by multiplying by $\cos m\phi$ or $\sin m\phi$.

2.2.1. Components of the electric current density. As in the earlier case of the SRC, we again start by specifying the volume electric current density, which is the sum of the drift current $\mathbf{j}_d$, the magnetization current $\mathbf{j}_m$, and the Birkeland current $\mathbf{j}_B$. Owing to the assumption that the background magnetic field $\mathbf{B}_0$ is purely dipolar, all three components of the current are expressed in a simple analytical form. The drift part of the current reads

$$\mathbf{j}_d = \frac{2cp(\alpha,\phi)}{B_0^3}\mathbf{B}_0 \times \nabla B_0 = -\frac{6c\sin\theta(1+\cos^2\theta)R^2 p(\alpha,\phi)}{M(1+3\cos^2\theta)^2}\mathbf{e}_\phi\ , \tag{15}$$

where c, M, and $\mathbf{e}_\phi$ are the speed of light, Earth's dipole moment, and the unit azimuthal vector, respectively. The magnetization current is

$$\mathbf{j}_m = c\,\nabla\times\left(-\frac{p}{B_0^2}\mathbf{B}_0\right) = -\frac{cr^2}{M(1+3\cos^2\theta)}\left\{\frac{\partial p}{\partial\phi}\mathbf{e}_r - 2\cot\theta\frac{\partial p}{\partial\phi}\mathbf{e}_\theta + \left[\frac{\partial p}{\partial\alpha}\frac{1+3\cos^2\theta}{r} - 6p\frac{1+\cos^2\theta}{1+3\cos^2\theta}\right]\mathbf{e}_\phi\right\}\ , \tag{16}$$

and the Birkeland current, obtained by integrating the divergence of the drift current (equation (15)) along the field line, reads (T93)

$$\mathbf{j}_B = \frac{6c}{M}\frac{\sqrt{1+3\cos^2\theta}}{\alpha^2\sin^6\theta}I(\cos\theta)\frac{\partial p}{\partial\phi}\frac{\mathbf{B}_0}{B_0}\ , \tag{17}$$

where

$$I(x) = \frac{1}{243}\left(\frac{27}{7}x^7 - \frac{99}{5}x^5 + \frac{117}{3}x^3 - 13x + \frac{256x}{1+3x^2}\right)\ . \tag{18}$$

Note that (17) and (18) provide an exact solution for the Birkeland current, driven by the divergence of the drift current in the case of nearly isotropic plasma, trapped in a purely dipolar magnetic field. Another simplifying assumption we made so far was the low-beta approximation, that is, the own field of the PRC was neglected.

2.2.2. Pressure and electric current distribution in the PRC model. Following the assumptions made in the beginning of section 2.2, the isotropic pressure was specified as a simple bell-shaped function of the parameter α and the longitude ϕ ($\phi = 0$ at noon):

$$p = \begin{cases} p_0\cos^2\left[\dfrac{\pi}{2}\dfrac{\alpha-\alpha_0}{\Delta\alpha}\right](\epsilon_1+\epsilon_2\cos\phi) & |\alpha-\alpha_0| \le \Delta\alpha\ , \\ 0 & |\alpha-\alpha_0| > \Delta\alpha\ . \end{cases} \tag{19}$$

Here the parameters α_0 and $\Delta\alpha$ give the position of the max-

imum of the pressure and the spread of the PRC across the dipolar L shells, respectively. These parameters, in turn, are defined by the equatorial (e) and polar (p) colatitudes of the PRC boundaries at the ionospheric level, assumed in this particular model as $\theta_e = 62^\circ$ and $\theta_p = 70^\circ$. Accordingly,

$$\alpha_0 = \frac{\alpha_e + \alpha_p}{2}, \qquad \Delta\alpha = \frac{\alpha_e - \alpha_p}{2}, \tag{20}$$

where $\alpha_{e,p} = \sin^2\theta_{e,p}$. The local time variation of the pressure function (equation (19)) is contained in the factor $\epsilon_1 + \epsilon_2 \cos\phi$.

Setting $\epsilon_1 = 1$ and $\epsilon_2 = 0$ and substituting (19) into (15)–(17) yields the axisymmetric part of the PRC (a purely azimuthal current with $\mathbf{j}_B = 0$). In the opposite case, $\epsilon_1 = 0$ and $\epsilon_2 = 1$, we obtain a quadrupole current system, consisting of the field-aligned currents, having the sense of the Region 2, and their distant azimuthal closure currents at low latitudes, flowing in opposite directions in the day and night sectors near the equator. Adding together these two current systems yields the desired model PRC, in which the axisymmetric and quadrupole currents cancel each other on the dayside and double the net current on the nightside at low latitudes, so that all Birkeland currents are fed by the nightside drift current (see Figure 1 in T93). Figure 8 shows a plot of the pressure distribution in the midnight meridional cross section of the model PRC, confined between the L shells with the equatorial radii 4.54 and 8.55 R_E (corresponding to the adopted values of $\theta_e = 62^\circ$ and $\theta_p = 70^\circ$). Figure 9 displays the pattern of the azimuthal electric current density in the same meridional plane.

Note again that the pressure profile in Figure 8 represents only the PRC and does not include the contribution from the plasma sheet particles. This is why the assumed $p(\alpha, \phi)$ falls to zero at the outer boundary of the PRC; in actuality, the PRC particle population smoothly merges with that of the plasma sheet, so that the total pressure decreases significantly slower. This also implies that the actual area of the generation of the Region 2 currents extends to larger distances on the nightside than we have assumed in this model. In this regard, it is interesting to evaluate the total magnitude of the model field-aligned current. This can be done using the continuity of the total current, by integrating the azimuthal current flowing across the midnight meridian plane. Since the azimuthal component of the PRC is zero at noon, all the azimuthal current flowing on the nightside should close via the ionosphere. For the above assumed values of the model parameters the total azimuthal current on the nightside (including both axisymmetric and quadrupole parts) was found equal to 0.7 MA. Owing to the north-south symmetry, this current is equally divided into Birkeland currents, flowing into the northern and southern ionospheres, so that the net downward current in each hemisphere is 0.35 MA. Since we assumed $p_0 = 1$nPa both for the symmetrical and for the quadrupole parts of the model PRC, the total noon-midnight pressure variation is $\Delta p = p_{\text{midn}} - p_{\text{noon}} = 2$ nPa, and hence the net downward field-aligned current per $\Delta p = 1$ nPa is 0.175 MA. According to *Iijima et al.* [1978], during relatively quiet periods the total Region 2 field-aligned current at low altitudes amounts to at least $\sim$ 1 MA, which requires the noon-midnight pressure asymmetry $\Delta p \sim 6$ nPa in our model. This is much larger than $\Delta p \sim 1$ nPa, following from the quiet time data of LH92 (and confirmed in another study by *De Michelis et al.* [1999]). It is unlikely that the discrepancy can be attributed to the assumption of a purely dipolar field; to make this point clearer, let us make another order-of-magnitude estimate.

As said above, in the model PRC the total downward field-aligned current I per each hemisphere is equal to the total azimuthal current in the axisymmetrical part of the PRC. This current can be independently evaluated using the formula of Dessler-Parker-Sckopke and assuming that all the current flows in a thin circular loop of a radius R:

$$\frac{2W}{M} = \frac{2\pi I}{cR},$$

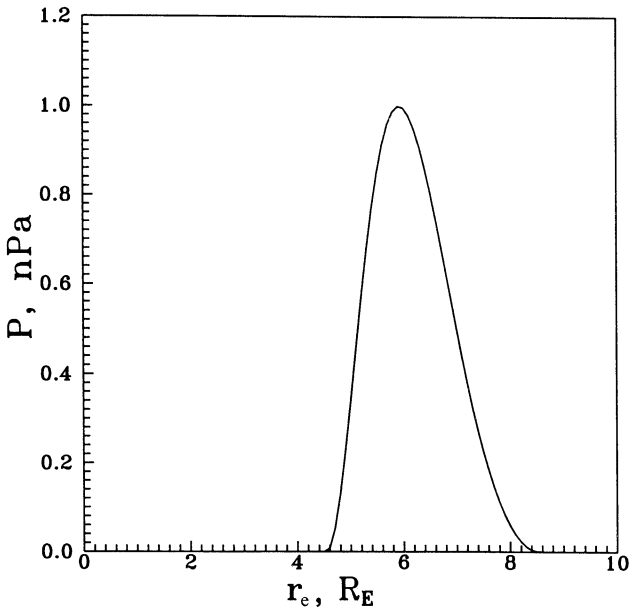

Figure 8. Equatorial radial profile of the isotropic pressure in the model partial ring current. Owing to the assumed isotropy, the pressure is constant along the dipolar field lines, and its local time variation is contained in the factor $\epsilon_1 + \epsilon_2 \cos\phi$.

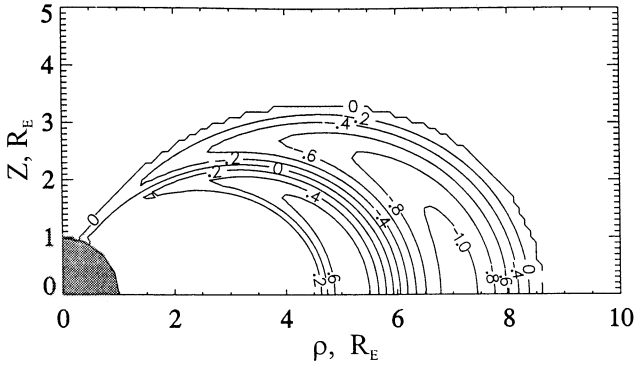

Figure 9. Distribution of the azimuthal component of the volume current density j in the model partial ring current (PRC), obtained from equations (15), (16), and (19) in the midnight meridian plane. The lines of equal intensity of j are labeled in nanoamperes per square meter.

where W is the total energy of particles in the axisymmetrical part of the PRC and M is the Earth's magnetic moment. The average energy density w can then be estimated by dividing W by the volume V of the model PRC, and to obtain its noon-midnight variation, one needs just to double the result, in order to take into account the contribution of the quadrupole term: $\Delta w = 2w$. Finally, the pressure asymmetry is $\Delta p = (2/3)\Delta w$. This results in a simple formula,

$$\Delta p = 2.04 \cdot 10^4 \frac{I}{RV},$$

where the pressure asymmetry Δp is in nanopascals, the total Birkeland current I is in mega-amperes, and the radius R and the volume V of the PRC are in R_E and R_E^3, respectively. In our model, $V \approx 500\ R_E^3$ and $R \sim 6\ R_E$. Assuming $I = 1$ MA, we obtain $\Delta p \approx 6.8$ nPa, which is fairly close to the previous estimate.

As was shown by *Sckopke* [1972], taking into account the nonlinear effects of the ring current field does not result in a significant modification of the total energy stored in the ring current and hence in its net magnetic effect. In particular, a correction term W_m in the Dessler-Parker-Sckopke relation, representing the magnetic energy of the ring current itself, becomes largely offset by a significant decrease of the kinetic energy term W due to a spatial restructuring of the magnetic field. Therefore we are forced to conclude that, at least during quiet conditions, the field-aligned current, associated with the noon-midnight asymmetry of the ring current, represents a relatively small part of the total Region 2 current, and hence most of that current actually comes from the near-Earth plasma sheet.

It is interesting to visualize a three-dimensional (3-D) configuration of the PRC, which in our case, in contrast to that in T93, extends over a significant interval of the radial distance. Figure 10 shows 3-D views of four families of flow lines of the total electric current, crossing the midnight meridian plane along four dipolar field lines with equatorial radii $R_e = 7.5$, 7.0, 6.5, and 6.0 R_E. Among the current flow lines the ones whose midnight crossing points lie on the outermost L shell usually reach the ionosphere as Birkeland currents. However, for smaller values of R_e, the current lines at low latitudes do not reach the ionosphere but close at smaller distances. This is owing to the effect of the magnetization current, which flows across the magnetic field and encircles the region of the largest particle pressure, resulting in a radial component of **j** in the dawn and dusk sectors and in an eastward current in the inner region on the nightside. This is especially clearly seen in the bottom right panel of Figure 10

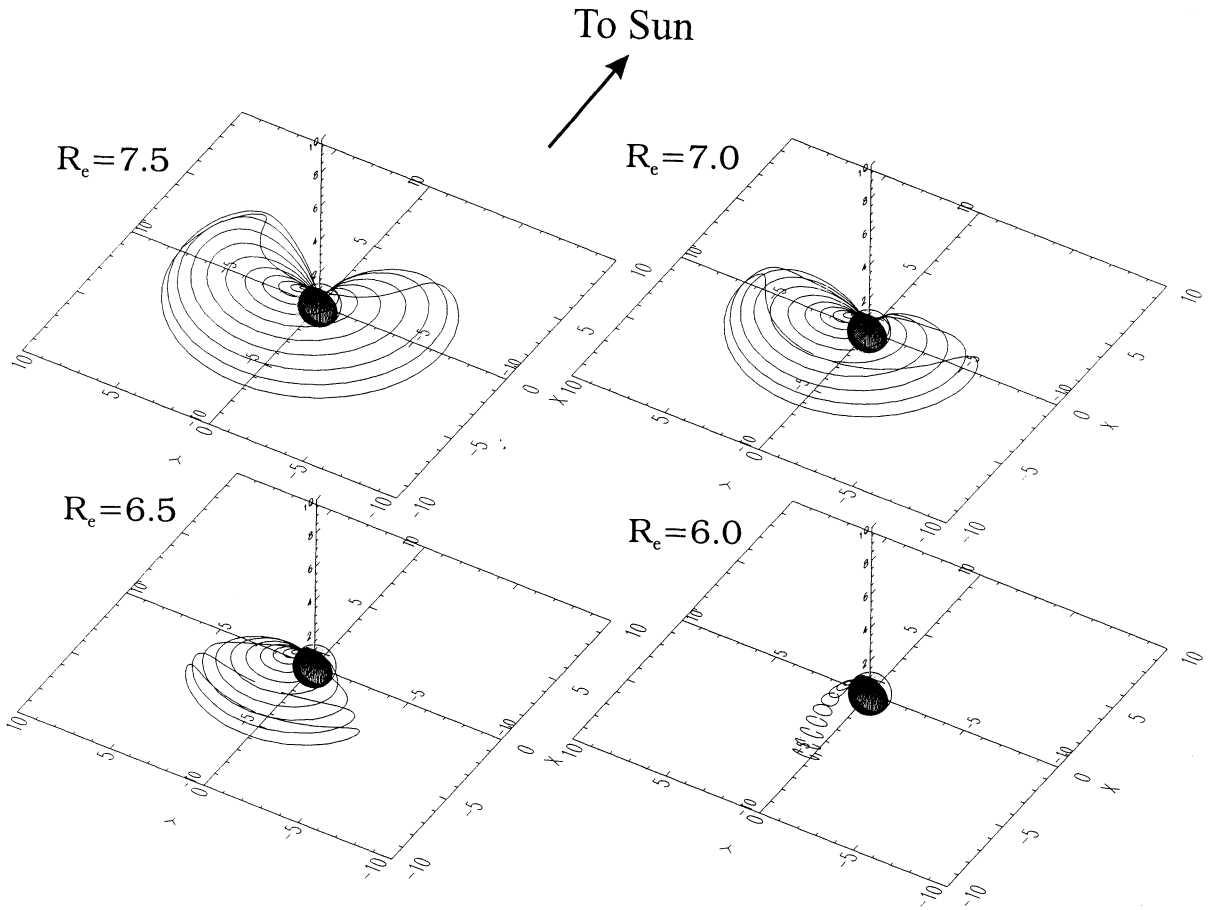

Figure 10. Views of electric current flow lines in the model partial ring current (PRC). The lines of **j** in each of the four panels cross the midnight meridian plane at points lying on the same dipolar field lines, whose equatorial radii R_e are labeled near each plot. Owing to the local time variation of the pressure, the current flow lines encircle the region of the peak pressure at midnight, owing to the magnetization component of **j**.

for $R_e = 6.0$. (In a similar way, flow lines of the magnetization current encircle the funnels of high plasma pressure in the polar cusps.)

2.2.3. Magnetic field of the model PRC. The next step is to calculate the magnetic field of the PRC by taking the Biot-Savart integral over the above defined current distribution and then devising a suitable analytical approximation for it. Because of the different structure of the axially symmetric and quadrupole components of the PRC, it is convenient to derive them separately, using two different methods. The axisymmetric part is modeled in exactly the same way as the SRC field in section 2.1, that is, by the azimuthal component A_ϕ of a vector potential of a pair of spread-out current loops, modified by a best fit deformation of the dipolar coordinates α and γ, which makes the analytically approximated A_ϕ as close as possible to that obtained from the Biot-Savart integral.

Modeling of the quadrupole part of the PRC seems less straightforward, because it lacks the axial symmetry, and hence at least two components of the vector potential are needed. Fortunately, the cosine dependence of the pressure on the azimuthal angle ϕ again proves very helpful. Namely, as shown in T93 (Appendix B), in this case all three spherical components of **B** assume a simple form:

$$\begin{aligned} B_r(r,\theta,\phi) &= b_r(r,\theta)\cos\phi\,, \\ B_\theta(r,\theta,\phi) &= b_\theta(r,\theta)\cos\phi\,, \\ B_\phi(r,\theta,\phi) &= b_\phi(r,\theta)\sin\phi\,, \end{aligned} \tag{21}$$

with the azimuthal dependence represented by the factors $\sin\phi$ and $\cos\phi$. Substituting the field components of (21) into the equation $\nabla \cdot \mathbf{B} = 0$ in spherical coordinates allows one to express the azimuthal component B_ϕ via B_r and B_θ as

$$B_\phi = -\left[\frac{\sin\theta}{r}\frac{\partial}{\partial r}\left(r^2 b_r\right) + \frac{\partial}{\partial\theta}\left(\sin\theta\, b_\theta\right)\right]\sin\phi\,. \tag{22}$$

In other words, zero divergence can be assured without having to resort to the vector potential, and it suffices to numerically calculate and find analytical approximations for b_r and b_θ in only one meridional plane (e.g., for $\phi = 0$) and then to obtain from (21) and (22) B_ρ, B_θ, and B_ϕ in the entire space.

The Biot-Savart integration procedure adopted for the PRC was essentially the same as the one for the SRC, described in section 2. The only noteworthy difference regards the Birkeland current closure in the ionosphere, a question discussed in more detail in section 2.2.3.2.

2.2.3.1. Axisymmetric part of the PRC and its analytical approximation: Figure 11 shows the numerically calculated distribution of the azimuthal component A_ϕ of the vector potential for the axisymmetrical component of the PRC, obtained from (15)–(19) with $\epsilon_1 = 1$ and $\epsilon_2 = 0$. The peak value p_m of the pressure in (19) was assumed equal to 1 nPa. This parameter controls the overall strength of the PRC and hence the degree of the asymmetry of the entire ring current, which depends on the state of the magnetosphere and should be derived from data. Therefore the assumed $p_m = 1$ nPa is just an arbitrary reference value, corresponding to a model PRC of unit strength.

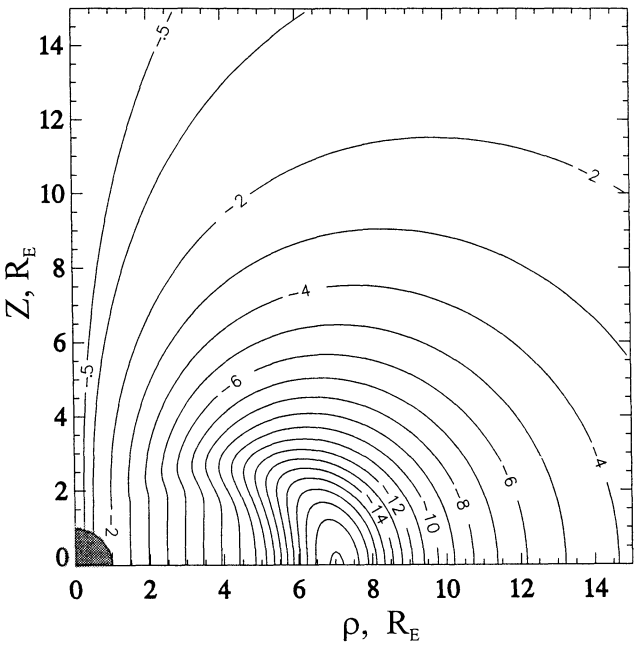

Figure 11. Distribution of the numerically computed azimuthal component A_ϕ of the vector potential, corresponding to the axially symmetrical component of the model PRC. The lines of equal A_ϕ are labeled in units nT·R_E.

The finally adopted representation for the magnetic field of the axisymmetric part of the PRC employs a two-term vector potential, mathematically identical to that given by (10) for the model SRC (not duplicated here), with the deformed coordinates ρ and z. The choice of the deformation, however, was not as simple as for the SRC model, described in section 2.1. Because of the assumed isotropic pressure, the azimuthal currents extend much farther away from the equator than in the SRC model (compare Figure 9 with the middle panel of Figure 3), which results in a more complex pattern of A_ϕ (compare Figures 11 and 4).

This made necessary a more sophisticated analytical approximation. In particular, instead of the coordinates r and θ used in the deformation (equation (11)), it proved more efficient to use the undeformed dipolar coordinates α and γ, since the PRC particle distribution is relatively narrow in the radial direction and rather extended along the dipolar field lines. Also, to achieve a decently accurate approximation, it was found necessary to deform both α and γ coordinates (while in the case of the SRC it sufficed to deform only α) and include more expansion terms. The finally adopted deformation reads as follows:

$$\alpha' = \alpha\left\{1 + \frac{p_1 \exp\left[-\left(\frac{\gamma}{\Delta\gamma_1}\right)^2\right]}{\left[1+\left(\frac{\alpha-\alpha_1}{\Delta\alpha_1}\right)^2\right]^{\beta_1}} + \sum_{n=2}^{3}\frac{p_n(\alpha-\alpha_n)^{n-1}}{\left[1+\left(\frac{\alpha-\alpha_n}{\Delta\alpha_n}\right)^2\right]^{\beta_{2n-2}}\left[1+\left(\frac{\gamma}{\Delta\gamma_n}\right)^2\right]^{\beta_{2n-1}}}\right\}, \tag{23}$$

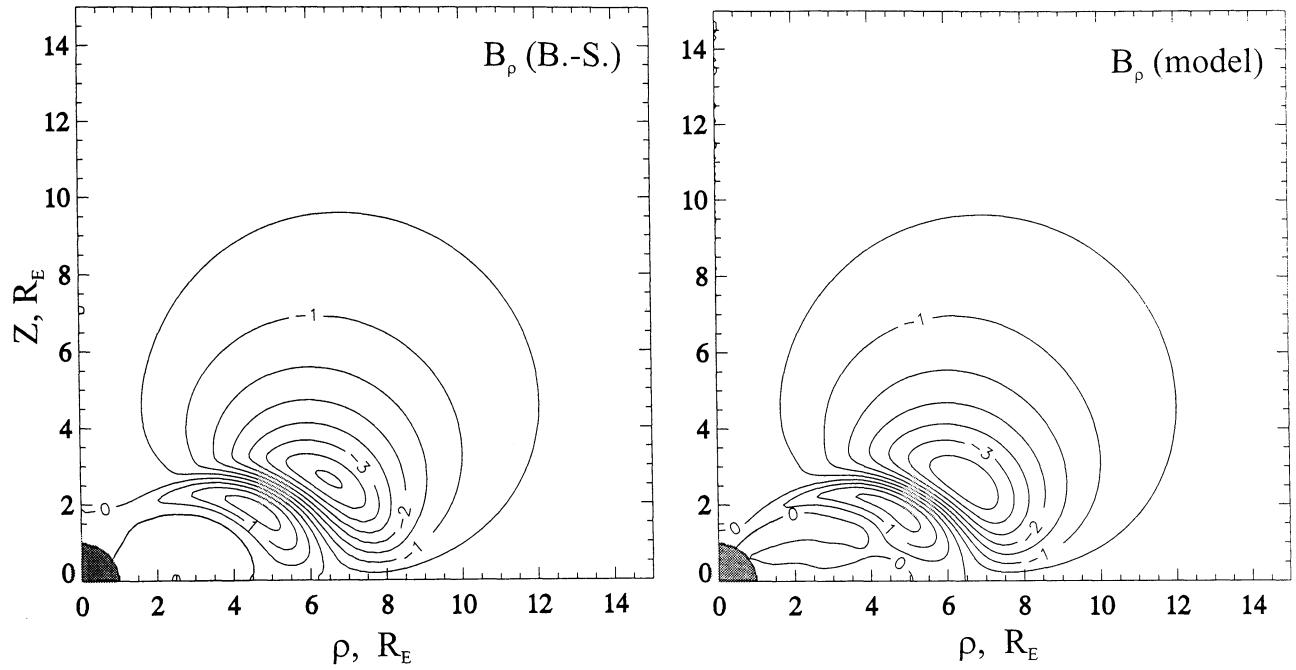

Figure 12. Comparison of the magnetic fields, obtained from the numerically computed axially symmetric vector potential (left), with those derived from the model approximation (equations (10), (23), and (24)) (right). These plots correspond to the B_ρ component of the field, and the lines of equal intensity are labeled in nanotesla.

$$\gamma' = \gamma\left\{1 + q_0 + q_1(\alpha-\alpha_4)\exp\left[-\left(\frac{\alpha-\alpha_4}{\Delta\alpha_4}\right)^2 - \left(\frac{\gamma}{\Delta\gamma_4}\right)^2\right] + \frac{q_2(\alpha-\alpha_5)}{\left[1+\left(\frac{\alpha-\alpha_5}{\Delta\alpha_5}\right)^2\right]^{\beta_6}\left[1+\left(\frac{\gamma}{\Delta\gamma_5}\right)^2\right]^{\beta_7}}\right\}. \quad (24)$$

The total number of the parameters here is 34, including 6 parameters of the current loops (a_1, a_2, ρ_1, ρ_2, D_1, and D_2) entering in (10) and 28 deformation parameters in (23) and (24). Their best fit values are given in Table 1; the corresponding rms error was found as low as $\sigma = 0.3\%$. Figures 12 and 13 compare the distributions of the magnetic field components B_ρ and B_z (in cylindrical coordinates), computed by

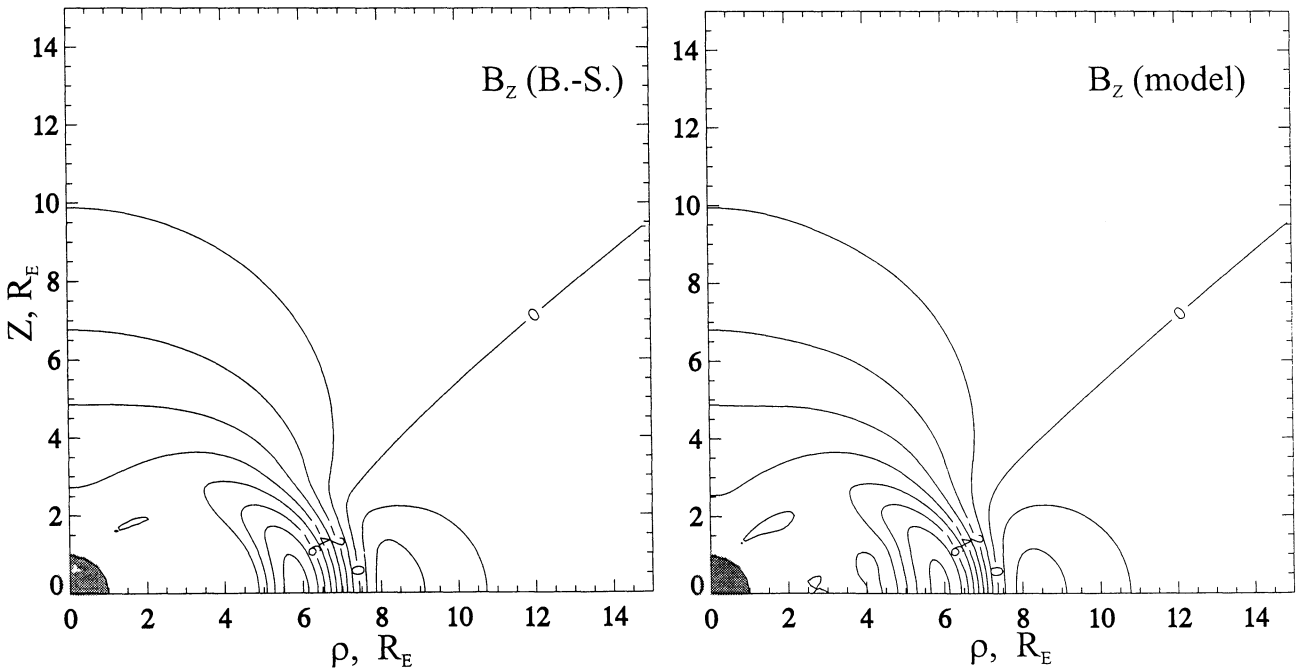

Figure 13. Same as Figure 12 but for the B_z component.

the Biot-Savart integral, with those obtained from the model. As expected from the highly accurate fitting of the vector potential, the two magnetic fields are also very similar.

2.2.3.2. The quadrupole part of the PRC and its analytical approximation: In contrast to the axisymmetric ring currents (SRC and the first component of the PRC) the Biot-Savart integral for the quadrupole part includes contributions from the field-aligned currents, which should be properly closed at ionospheric altitudes. The actual geometry of the closure depends on the distribution of the ionospheric conductivity, but, owing to the relatively small scale of the ionospheric currents, the details of that closure have an appreciable effect only within a few thousand kilometers above the ionosphere, in regions where the Earth's main field exceeds that of the Birkeland currents by at least a factor of 100. For the purposes of the global magnetospheric modeling, a simple approximation for the closure current is quite sufficient, based on a uniform ionospheric conductivity and on the assumption of the symmetry of the Birkeland currents with respect to the equatorial, noon-midnight, and dawn-dusk meridian planes.

In this scenario, for any field-aligned current $\Delta\mathbf{j}$, flowing into the ionosphere over a small area of the ionosphere, there exists an equal current, flowing out of the ionosphere in the antipodal point. Owing to the uniform conductivity, the closure currents for this pair of elementary Birkeland currents will flow along the meridians, connecting the inflow and outflow areas, and their integral magnetic effect above the ionosphere will be equivalent to that of the straight segment of the electric current, connecting the inflow and outflow points and passing through the Earth's center. This method of closing the Birkeland current was used in the present work.

Figure 14 shows the plots of the quadrupole B_r and B_θ components in the noon meridian plane ($\phi = 0$), obtained by the Biot-Savart integral. To have the best fit field faithfully represent the highly structured patterns required somewhat sophisticated expansions. To approximate the sharp "ridges" and kink-like features, conspicuous in the vicinity of the field-aligned currents, it was found helpful to use the functions

$$f_1(\alpha, \alpha_0, \Delta\alpha) = \frac{2\alpha}{S_+ + S_-}\,, \quad f_2 = f_1/\alpha\,, \quad f_3 = \frac{df_1}{d\alpha}\,, \tag{25}$$

where

$$S_+ = \sqrt{(\alpha + \alpha_0)^2 + \Delta\alpha^2}\,, \quad S_- = \sqrt{(\alpha - \alpha_0)^2 + \Delta\alpha^2}\,,$$

which allowed us to obtain accurate and economical approximations for both b_r and b_θ. Before writing down the field components, note that owing to the symmetry, $b_r = 0$ at the polar axis ($\theta = 0$) and in the equatorial plane ($\theta = \pi/2$); therefore it is convenient to incorporate this behavior from the outset by using an auxiliary variable b_r^*, defined through $b_r = b_r^* \sin\theta\cos\theta$.

After having explored many possible approximations, the following simple and accurate expansions for b_r^* and b_θ were chosen:

$$\begin{aligned} b_r^* = &\sum_{n=1}^{3} \frac{\alpha^{\sigma_n} f_{k_n}^{\tau_n}(\alpha, \alpha_n, \Delta\alpha_n)}{(r/d_n)^{\beta_n} + 1}(a_{2n-1} + a_{2n}\cos^2\theta) \\ &+ \sum_{m=1}^{2}\sum_{n=1}^{4} \frac{a_{4m+n+2}}{\left[1 + \left(\frac{\alpha - \alpha_{m+3}}{\Delta\alpha_{m+3}}\right)^2\right]^n \left(1 + \frac{\gamma^2}{\Delta\gamma_m^2}\right)} \\ &+ \sum_{n=1}^{3} \frac{a_{n+14}\cos^{2n-2}\theta}{r^4 + c_n^4} + \frac{a_{18} f_3(\alpha, \alpha_6, \Delta\alpha_6)}{1 + \left(\frac{r - r_1}{\Delta r}\right)^2}\,, \end{aligned} \tag{26}$$

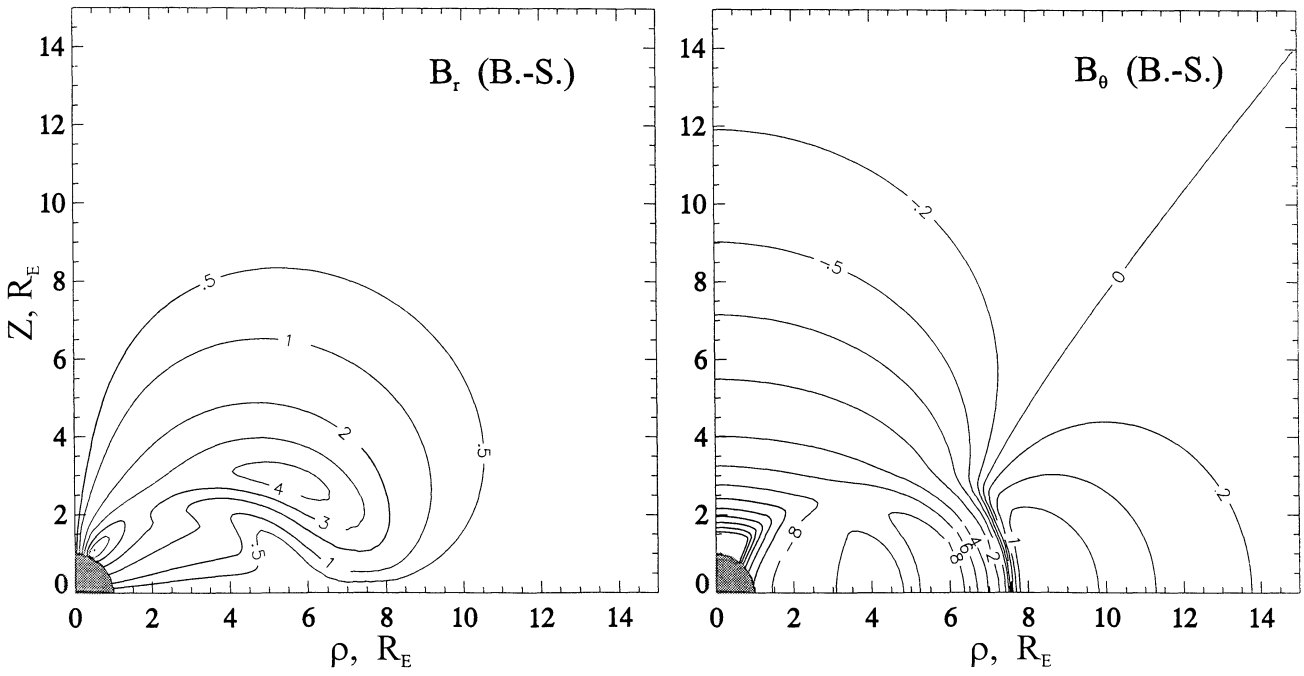

Figure 14. Distribution of B_ρ and B_θ components of the quadrupole part of the model PRC in the noon meridian plane, obtained by numerical evaluation of the Biot-Savart integral.

Table 1. Parameters of the Ring Current in Equations (10)–(12), (23) and (24), (26) and (27)

RC (symmetric): α'[a]		PRC (symmetric): α' and γ'[b]		PRC (quadrupole): b_r^*[c]		PRC (quadrupole): b_θ[d]	
Parameter	Value	Parameter	Value	Parameter	Value	Parameter	Value
a_1	-563.372	a_1	-801.120	a_1	-21.26663	a_1	12.74640
a_2	425.089	a_2	125.825	a_2	32.24527	a_2	-7.516394
ρ_1	4.15059	ρ_1	6.56049	a_3	-6.062894	a_3	-5.476234
ρ_2	3.33450	ρ_2	3.82721	a_4	7.515661	a_4	3.212705
D_1	2.26615	D_1	1.93071	a_5	233.7341	a_5	-59.10926
D_2	3.07907	D_2	0.77900	a_6	-227.1196	a_6	46.62198
p_1	0.0260243	p_1	0.305831	a_7	8.483234	a_7	-.0164428
r_1	8.93779	α_1	0.181714	a_8	16.80643	a_8	.1234229
Δr_1	3.32793	$\Delta\alpha_1$	0.125753	a_9	-24.63534	a_9	-.08579199
c_1	4.96679	β_1	3.42261	a_{10}	9.0671206	a_{10}	.01321367
p_2	0.0912583	$\Delta\gamma_1$	0.0474294	a_{11}	-1.052687	a_{11}	.8970494
r_2	6.24303	p_2	-4.80046	a_{12}	-12.08385	a_{12}	9.136186
Δr_2	1.750146	α_2	-0.0284564	a_{13}	18.61970	a_{13}	-38.19301
c_2	5.71796	$\Delta\alpha_2$	0.218811	a_{14}	-12.71686	a_{14}	21.73776
p_3	0.061067	β_2	2.54594	a_{15}	47017.36	a_{15}	-410.0783
r_3	2.07991	$\Delta\gamma_2$	0.00813273	a_{16}	-50646.71	a_{16}	-69.90833
Δr_3	0.682855	β_3	0.358682	a_{17}	7746.058	a_{17}	-848.8543
c_3	0.000000	p_3	103.160	a_{18}	1.531069	τ_1	1.243288
		α_3	-0.00764731	τ_1	2.318824	α_1	.2071721
		$\Delta\alpha_3$	0.104649	α_1	.1417519	$\Delta\alpha_1$	.05030555
		β_4	2.95886	$\Delta\alpha_1$	.006388013	d_1	7.471332
		$\Delta\gamma_3$	0.01172314	d_1	5.3039345	β_1	3.180534
		β_5	0.438287	β_1	4.213397	τ_2	1.376744
		q_0	0.0113491	τ_2	.7955534	τ_2	.1568504
		q_1	14.5134	α_2	.1401143	$\Delta\alpha_2$	.02092911
		α_4	0.264710	$\Delta\alpha_2$	.02306094	β_2	1.985148
		$\Delta\alpha_4$	0.0709123	d_2	3.462235	τ_3	.31571399
		$\Delta\gamma_4$	0.0151296	β_2	2.5687430	σ_3	1.056300
		q_2	6.86132	σ_3	3.477426	α_3	.1701395
		α_5	0.167740	τ_3	1.922155	$\Delta\alpha_3$	.1019870
		$\Delta\alpha_5$	0.0443365	α_3	.1485233	d_3	6.293741
		$\Delta\gamma_5$	0.0555374	$\Delta\alpha_3$	.02319676	β_3	5.671824
		β_6	0.766560	d_3	7.830224	α_4	.1280772
		β_7	0.727785	β_3	8.492933	$\Delta\alpha_4$	.02189061
				α_4	.1295222	$\Delta\gamma_1$	.01040696
				$\Delta\alpha_4$	.01753009	α_5	.1648266
				$\Delta\gamma_1$	.01125504	$\Delta\alpha_5$	.04701593
				α_5	.1811846	$\Delta\gamma_2$	.01526400
				$\Delta\alpha_5$	.04841237	c_1	3.589407
				$\Delta\gamma_2$	.01981805	c_2	1.833514
				c_1	6.557802	c_3	4.841667
				c_2	6.348576	d_2	1.0[e]
				c_3	5.744437	σ_1	0.0[e]
				α_6	.2265213	σ_2	0.0[e]
				$\Delta\alpha_6$	.1301957		
				Δr	.5654023		
				σ_1	0.0[e]		
				σ_2	0.0[e]		
				r_1	1.2[e]		

[a]Parameters for axisymmetric ring current (RC) from equations (10)–(12).
[b]Parameters for axisymmetric part of the partial RC (PRC) from equations (23) and (24).
[c]Parameters for quadrupole part of the PRC from equation (26).
[d]Parameters for quadrupole part of the PRC from equation (27).
[e]Fixed parameter

where $k_n = 1$ for $n = 1, 2$ and $k_n = 3$ for $n = 3$;

$$b_\theta = \sum_{n=1}^{3} \frac{\alpha^{\sigma_n} f_n^{\tau_n}(\alpha, \alpha_n, \Delta\alpha_n)}{(r/d_n)^{\beta_n} + j_n}(a_{2n-1} + a_{2n}\cos^2\theta)$$
$$+ f_3(\gamma, 0, \Delta\gamma_1)\sum_{n=1}^{4} \frac{a_{n+6}}{\left[1 + \left(\frac{\alpha - \alpha_4}{\Delta\alpha_4}\right)^2\right]^n}$$
$$+ \sum_{n=1}^{4} \frac{a_{n+10}}{\left[1 + \left(\frac{\alpha - \alpha_5}{\Delta\alpha_5}\right)^2\right]^n \left(1 + \frac{\gamma^2}{\Delta\gamma^2}\right)}$$
$$+ \sum_{n=1}^{3} \frac{a_{n+14}\cos^{2n-2}\theta}{r^4 + c_n^4}, \qquad (27)$$

and where $j_n = 1$ for $n = 1, 3$ and $j_n = 0$ for $n = 2$. The best fit values of the parameters entering in (26) and (27) are given in Table 1.

It should be noted that even though from a formal viewpoint there is no need to numerically calculate and separately approximate the azimuthal component b_ϕ, the problem is actually not that simple. Because of the derivatives in the right-hand side of (22), even small inaccuracies in the approximations for b_r and b_θ result in relatively large deviations of b_ϕ from the exact solution. To minimize this effect, the derivation of the parameters in (26) and (27) was performed in two steps.

First of all, a separate fitting was made of b_r and b_θ to the corresponding exact distributions, obtained from the Biot-Savart integral. The obtained values of the parameters were then used as starting guesses for the next round of iterations, in which all three components, b_r, b_θ, and b_ϕ, were fitted jointly, to minimize the sum of their individual merit functions $\sigma = \sigma_r + \sigma_\theta + \sigma_\phi$. This correction resulted in a dramatic increase of the accuracy of b_ϕ, at the expense of some increase in the values of σ_r and σ_θ: The relative rms error $\sigma_\phi/\langle b_\phi^2\rangle^{1/2}$ fell from ≈ 10 to $\approx 2.9\%$, while the rms errors for b_r and b_θ rose from ≈ 0.8 to $\approx 1.5\%$.

Figure 15 shows the model plots of b_r and b_θ in the same format as their exact distributions in Figure 14. Figure 16 compares three plots for b_ϕ: The one on the left shows the exact result from the Biot-Savart integral, the middle plot shows the distribution obtained from (22) using the individual fits for b_r and b_θ, and the plot on the right shows b_ϕ, corrected by the joint refitting of all three components.

3. Discussion and Concluding Comments

In this study a quantitative model was devised for the magnetic field of a realistic ring current, based on the observed quiet time distributions of the particle pressure and its anisotropy. The model reproduced the observed local time asymmetry of the outer ring current, significant already at $r \geq 5\,R_E$ and increasing with growing radial distance. The azimuthally asymmetric distribution of particle pressure gives rise to field-aligned currents having the sense of the Region 2; their magnetic field was also evaluated and was analytically represented in a single global model. The obtained approximations are rapidly derived by available desktop computers and are intended to be used in advanced data-based models of the inner magnetosphere, an important component of any space weather specification model.

Our several simplifying assumptions leave significant room for improvement of the model. First, in the calculation of the electric current density we used a purely dipolar background field, while the actual field can be significantly stretched on the nightside by the magnetic effects of both the ring current

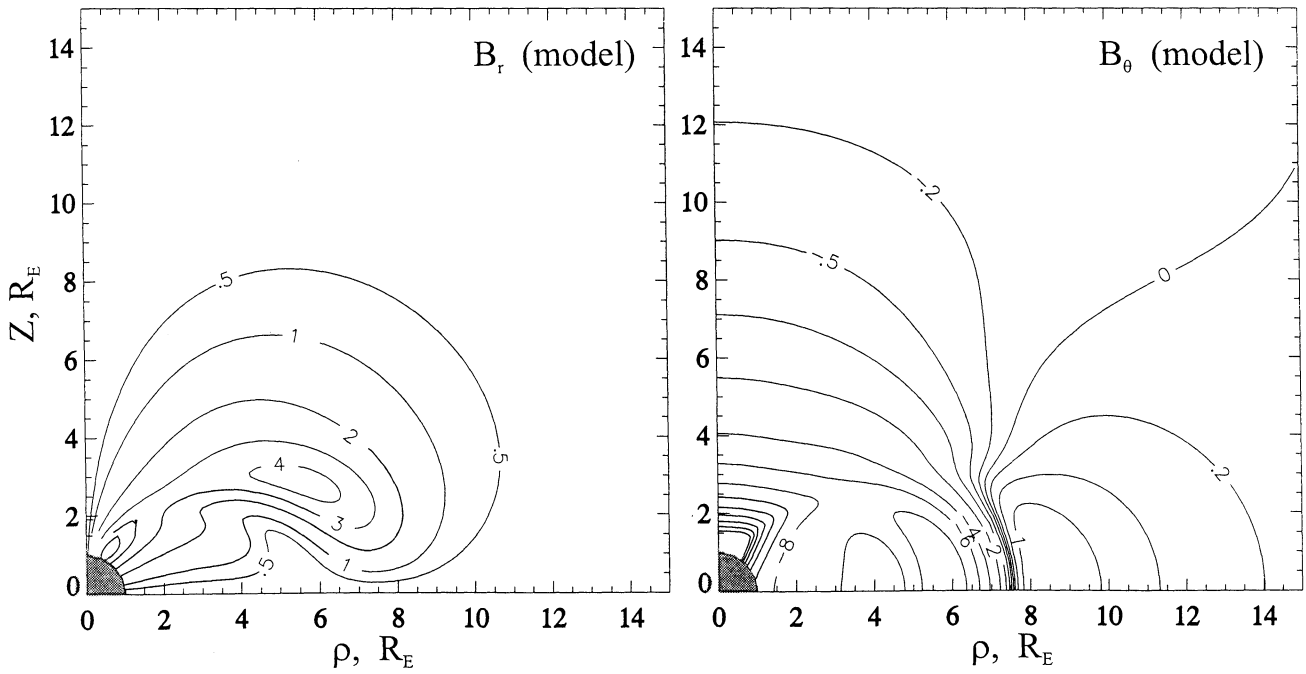

Figure 15. Distribution of B_ρ and B_θ components, similar to those in Figure 14 but obtained from the analytical approximation (equations (26) and (27)).

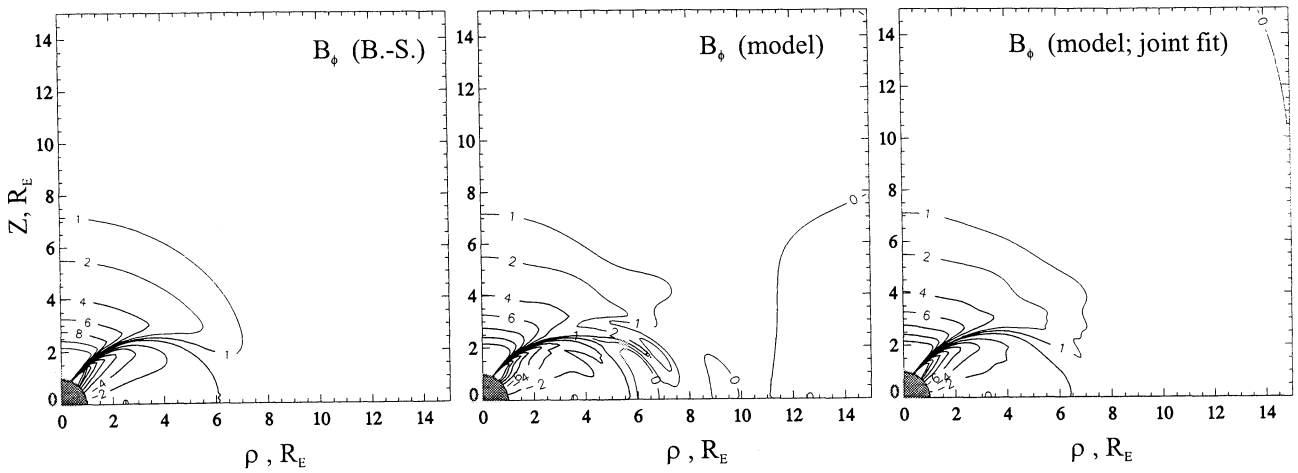

Figure 16. Distribution of the azimuthal component B_ϕ of the quadrupole part of the model PRC, (left) obtained by the Biot-Savart integral, (middle) derived from (22) using individual fits of equations (26) and (27) for b_r and b_θ, and (right) after a joint fit of all three components.

itself and the cross-tail current. This effect, observed even as close as the synchronous orbit [*Kaufmann,* 1987], produces an even stronger concentration of the current near the equatorial plane than the one obtained using the dipolar field. A straightforward modification of the above calculations using a more realistic background field would run into serious problems, caused by the breakdown of the axial symmetry of that field. In that case, expanding the axially asymmetric pressure function into the Fourier series in ϕ would no longer result in the separation of the azimuthal dependence and hence would force us to abandon the "quasi-2-D" approach and to resort to the full-scale 3D modeling. A much simpler way to incorporate the nondipolar geometry would be to apply appropriate deformations of the coordinates [*Stern,* 1987; *Tsyganenko,* 1998b], keeping in mind that the natural coordinates for the ring current are the dipolar ones, α and γ, which allow simple transformations to spherical/cylindrical coordinates and back, as specified in (13) and (14). The deformation technique also proves very helpful for representing the effects of the Earth's dipole tilt on the geometry of distant field sources, including the outer ring current and the inner cross-tail current on the nightside. Possible uses of the deformation method for further modifications of the model ring current go beyond the scope of this paper and will be addressed in a separate publication.

At low altitudes the total magnetic effect of the ring current should also include the induction field, produced by currents flowing inside the Earth, and the shielding field of the magnetopause currents. The first current system is important in modeling time-dependent ring current fields at and near the Earth's surface. It prevents the full penetration of the ring current disturbance field inside Earth and results in an enhancement of the negative H component at low latitudes. The second current flows on the magnetopause and confines the total field of the ring current within the magnetospheric boundary. Both effects can be easily taken into account, using the fact that by contrast to the field of the ring current itself, both the induction and shielding fields are curl-free inside the magnetosphere and can be represented there by a scalar potential.

Using the observed values of the noon-midnight asymmetry of the ring current particle pressure, an estimate was made of the contribution of the partial ring current to the Region 2 system of Birkeland currents. At least for quiet conditions, that contribution was found not to exceed $\sim$ 20% of the total Region 2 current, observed at low altitudes. This suggests the near-Earth plasma sheet as the main source of that current.

Of special importance is the modeling of the storm time ring current, distinguished by a dramatic increase in the energy density due to the injection of new particles and the energization of the previously existing population. The geometry of the storm time ring current is also different: Its peak shifts earthward, and it develops a strong dawn-dusk asymmetry with more depressed field on the duskside. These effects can, in principle, be replicated by a deformation of the model field; the simplest approach would be a spatial scaling of the ring current, combined with an appropriate modulation of its overall strength and a rotation of the PRC peak toward earlier local times.

The above subject is related to the more general and important problem of gauging principal physical processes that control the ring current: the injection of new energetic particles into the trapping region and their eventual loss. Since the ring current resides close to the Earth, where both the geomagnetic field and its gradient are quite large, the timescales involved range from several minutes to tens of hours. For that reason, not only the current solar wind conditions but also their earlier history are important. The problem of predicting the ring current state has been addressed in the past by means of numerical simulations [e.g., *Harel et al.*, 1981; *Fok et al.,* 1999] or by using an empirical approach, devised by *Burton et al.* [1975] and further developed by *Valdivia et al.* [1996] for a short-term forecast of the *Dst* index. These issues, however, extend beyond the scope of the present paper. Our goal here was to devise a mathematical framework, representing the global spatial structure of the magnetic field of the asymmetric ring current and of the associated field-aligned currents, without considering time-dependent processes. We also note that although the numerical fits were made here for only one pressure/anisotropy profile, obtained in LH92 for

quiet conditions, the above described method can, in principle, be used for a variety of particle distributions, observed at different periods.

Acknowledgments. The author is grateful to David Stern for his careful reading and numerous comments on the manuscript. Thanks are also due to Tony Lui for his discussion of the observed asymmetry of the ring current. This work is supported by NASA grants NAS5-32350 and NAS5-32993, and NSF Magnetospheric Physics Program grant ATM-9819873.

Janet G. Luhmann thanks Jean-Claude Kosik, Michael Schulz, and another referee for their assistance in evaluating this paper.

References

Akasofu, S.-I., and S. Chapman, The ring current, geomagnetic disturbance, and the Van Allen radiation belts, *J. Geophys. Res., 66,* 1321, 1961.

Burton, R. K., R. L. McPherron, and C. T. Russell, An empirical relationship between interplanetary conditions and *Dst*, *J. Geophys. Res., 80,* 4204, 1975.

Cowley, S. W. H., The effect of pressure anisotropy on the equilibrium structure of magnetic current sheets, *Planet. Space Sci., 26,* 1037, 1978.

Daglis, I. A., R. M. Thorne, W. Baumjohann, and S. Orsini, The terrestrial ring current: Origin, formation, and decay, *Rev. Geophys., 37,* 407, 1999.

De Michelis, P., I. A. Daglis, amd G. Consolini, An average image of proton plasma pressure and of current systems in the equatorial plane derived from AMPTE/CCE-CHEM measurements, *J. Geophys. Res., 104,* 28,615, 1999.

Fok, M.-C., T. E. Moore, and D. C. Delcourt, Modeling of inner plasma sheet and ring current during substorms, *J. Geophys. Res., 104,* 14,557, 1999.

Harel, M., R. A. Wolf, P. H. Reiff, R. W. Spiro, W. J. Burke, F. J. Rich, and M. Smiddy, Quantitative simulation of a magnetospheric substorm, 1, Model logic and overview, *J. Geophys. Res., 86,* 2217, 1981.

Hilmer, R. V., and G.-H. Voigt, A magnetospheric magnetic field model with flexible current systems driven by independent physical parameters, *J. Geophys. Res., 100,* 5613, 1995.

Hoffman, R. A., and P. A. Bracken, Magnetic effects of the quiet-time proton belt, *J. Geophys. Res., 70,* 3541, 1965.

Hoffman, R. A., and P. A. Bracken, Higher order ring currents and particle energy storage in the magnetosphere, *J. Geophys. Res., 72,* 6039, 1967.

Iijima, T., T. A. Potemra, and L. J. Zanetti, Large-scale characteristics of field-aligned currents associated with substorms, *J. Geophys. Res., 83,* 599, 1978.

Iijima, T., T. A. Potemra, and L. J. Zanetti, Large-scale characteristics of magnetospheric equatorial currents, *J. Geophys. Res., 95,* 991, 1990.

Kaufmann, R. L., Substorm currents: Growth phase and onset, *J. Geophys. Res., 92,* 7471, 1987.

Kendall, P. C., S. Chapman, S.-I. Akasofu, and P. N. Swartztrauber, The computation of the magnetic field of any axisymmetric current distribution, with magnetospheric applications, *Geophys. J. R. Astron. Soc., 11,* 349, 1966.

Kosik, J.-C., Quantitative magnetic field model including magnetospheric ring current, *J. Geophys. Res., 94,* 12,021, 1989.

Kosik, J.-C., A quantitative model of the magnetosphere with poloidal vector fields, *Ann. Geophys., 16,* 1557, 1998.

Lackner, K., Deformation of a magnetic dipole field by trapped particles, *J. Geophys. Res., 75,* 3180, 1970.

Lui, A. T. Y., and D. C. Hamilton, Radial profiles of quiet time magnetospheric parameters, *J. Geophys. Res., 97,* 19,325, 1992.

Lui, A. T. Y., R. W. McEntire, and S. M. Krimigis, Evolution of the ring current during two geomagnetic storms, *J. Geophys. Res., 92,* 7459, 1987.

Lui, A. T. Y., H. E. Spence, and D. P. Stern, Empirical modeling of the quiet time nightside magnetosphere, *J. Geophys. Res., 99,* 151, 1994.

Nakabe, S., T. Iyemori, M. Sugiura, and J. A. Slavin, A statistical study of the magnetic field structure in the inner magnetosphere, *J. Geophys. Res., 102,* 17,571, 1997.

Parker, E. N., Newtonian development of the hydromagnetic properties of ionized gases of low density, *Phys. Rev., 107,* 924, 1957.

Peroomian, V., L. R. Lyons, and M. Schulz, Inclusion of shielded Birkeland currents in a model magnetosphere, *J. Geophys. Res., 103,* 151, 1998.

Schield, M. A., Pressure balance between solar wind and magnetosphere, *J. Geophys. Res., 74,* 1275, 1969.

Sckopke, N., A study of self-consistent ring current models, *Cosmic Electrodyn., 3,* 330, 1972.

Sozou, C., and D. W. Windle, A self-consistent ring current in the Earth's dipole field, *Planet. Space Sci., 17,* 375, 1969.

Spence, H. E., M. G. Kivelson, and R. J. Walker, Static magnetic field models consistent with nearly isotropic plasma pressure, *Geophys. Res. Lett., 14,* 872, 1987.

Stern, D. P., Tail modeling in a stretched magnetosphere, 1, Methods and transformations, *J. Geophys. Res., 92,* 4437, 1987.

Stern, D. P., A simple model of Birkeland currents, *J. Geophys. Res., 98,* 5691, 1993.

Sugiura, M., Equatorial current sheet in the magnetosphere, *J. Geophys. Res., 77,* 6093, 1972.

Tsyganenko, N. A., A global analytical representation of the magnetic field produced by the Region 2 Birkeland currents and the partial ring current, *J. Geophys. Res., 98,* 5677, 1993.

Tsyganenko, N. A., Effects of the solar wind conditions on the global magnetospheric configuration as deduced from data-based field models, *Eur. Space Agency Spec. Publ., ESA SP-389,* 181, 1996.

Tsyganenko, N. A., Data-based models of the global geospace magnetic field: Challenges and prospects of the ISTP era, in *Geospace Mass and Energy Flow: Results From the International Solar-Terrestrial Physics Program, Geophys. Monogr. Ser., vol. 104,* edited by J. L. Horwitz, D. L. Gallagher, and W. M. Peterson, p. 371, AGU, Washington, D. C., 1998a.

Tsyganenko, N. A., Modeling of twisted/warped magnetospheric configurations using the general deformation method, *J. Geophys. Res., 103,* 23,551, 1998b.

Tsyganenko, N. A., and M. Peredo, Analytical models of the magnetic field of disk-shaped current sheets, *J. Geophys. Res., 99,* 199, 1994.

Tsyganenko, N. A., and D. P. Stern, Modeling the global magnetic field of the large-scale Birkeland current systems, *J. Geophys. Res., 101,* 27,187, 1996.

Tsyganenko, N. A., and A. V. Usmanov, Determination of the magnetospheric current system parameters and development of experimental geomagnetic field models based on data from IMP and HEOS satellites, *Planet. Space Sci., 30,* 985, 1982.

Tsyganenko, N. A., G. Le, C. T. Russell, and T. Iyemori, A study of the inner magnetosphere based on data of Polar, *J. Geophys. Res., 104,* 10,275, 1999.

Valdivia, J. A., A. S. Sharma, and K. Papadopoulos, Prediction of magnetic storms by nonlinear models, *Geophys. Res. Lett., 23,* 2899, 1996.

Voigt, G.-H., A mathematical magnetospheric model with independent physical parameters, *Planet. Space Sci., 29,* 1, 1981.

Williams, D. J., The Earth's ring current: Causes, generation, and decay, *Space Sci. Rev., 34,* 223, 1983.

N. A. Tsyganenko, Code 690.2, Laboratory for Extraterrestrial Physics, NASA Goddard Space Flight Center, Greenbelt, MD 20771. (kolya@nssdca.gsfc.nasa.gov)

(Received April 11, 2000; revised July 28, 2000;
accepted August 22, 2000.)